IEEE Access
Multidisciplinary | Rapid Review | Open Access Journal

IEEE PHOTONICS SOCIETY SECTION

Received 7 February 2023, accepted 21 February 2023, date of publication 24 February 2023, date of current version 1 March 2023.

Digital Object Identifier 10.1109/ACCESS.2023.3249102

RESEARCH ARTICLE

FDTD Investigation of Efficient and Robust Integration Between Si_3N_4 and Ge-Rich GeSi for Waveguide-Integrated Electro-Absorption Optical Modulators

NATDANAI KHONGPETCH[1], WORAWAT TRAIWATTANAPONG[1,2], SURASAK CHIANGGA[1], PICHET LIMSUWAN[3], AND PAPICHAYA CHAISAKUL[1]

[1]Department of Physics, Faculty of Science, Kasetsart University, Bangkok 10900, Thailand
[2]Department of Materials Science and Engineering, Massachusetts Institute of Technology, Cambridge, MA 02139, USA
[3]Department of Physics, Faculty of Science, King Mongkut's Institute of Technology Ladkrabang, Bangkok 10520, Thailand

Corresponding author: Papichaya Chaisakul (fscipac@ku.ac.th)

This research and innovation activity is funded by National Research Council of Thailand (NRCT), and Kasetsart University Research and Development Institute (KURDI): FF(KU)27.65.

ABSTRACT Si_3N_4 photonic integrated circuits have gain significant and rapid interest in different photonic applications thanks to its superior passive performance. Nevertheless, optical integration between Si_3N_4 and Ge-based optical components remains critically challenging especially for optical modulation. In this paper, via 3D-FDTD calculations we investigate the optical integration between Si_3N_4 and Ge-based waveguides using vertical coupling configuration employing amorphous Si (α-Si) as an optical bridge showing efficient and robust coupling efficiency, which can be maintained according to the tolerant analysis with respect to the variations in optical wavelengths and critical parameters of the coupling structure. In addition, with respect to the recent theoretically-optimized SOI waveguide-integrated and also laterally-coupled Si_3N_4 waveguide-integrated Ge-based optical modulators, we found that the studied coupling structure could be employed to enable a low-voltage Si_3N_4 waveguide-integrated Ge-based optical modulator with a competitive extinction ratio/insertion loss performance, increasing the prospect of Si_3N_4-based photonic integrated circuits for low-energy optical interconnects.

INDEX TERMS Waveguide, Si_3N_4, germanium, photonic integrated circuits.

I. INTRODUCTION

Silicon nitride (Si_3N_4) has recently gained significant attention in Si-compatible photonic monolithic integration. Si_3N_4 has a relatively-wide bandgap (~5 eV), low thermo-optics coefficients, flexible optical properties and fabrication technologies, and sufficiently-high refractive index contrast with SiO_2 [1], [2], [3], [4], [5], [6], [7]. These characteristics contribute to its potentials for compact and wideband operations with a relatively-low sensitivity to the fabrication variation. Low-loss Si_3N_4 optical waveguides on bulk Si substrate and fabrication tolerant Si_3N_4 wavelength multiplexing devices have been developed affirming the prospect of Si_3N_4 photonic integrated circuits [8], [9], [10]. In addition, several works have been promisingly performed to enable the deposition of high quality Si_3N_4 with thickness close to or even higher than 1 μm [11], [12], [13], [14], unlocking the Si_3N_4 potential usage from the visible to mid-infrared spectral range. Nevertheless, to develop functional Si_3N_4-based photonic integrated circuits, efficient and robust optical integration between Si_3N_4 and Si-based active photonic components is also required. Among several Si-compatible options [15], Ge-based active devices are highly regarded for its ability to render optical detection, modulation, and emission on

The associate editor coordinating the review of this manuscript and approving it for publication was Leo Spiekman.

Si substrate together with its compatibility with top-down Si-CMOS fabrication processes [16], [17], [18], [19]. Therefore, although the optical integration between Si_3N_4 ($n \sim 2$) and Ge ($n \sim 4.3$) can be challenging due to the large refractive index difference, significant works have been performed in order to integrate Si_3N_4 passive optical waveguides with active Ge-based optical components. In particular, the optical integration between silicon nitride waveguides and Ge-on-Si photodetectors has been investigated both experimentally and theoretically [20], [21], [22]. The optical integration is based on the evanescent wave coupling from the silicon nitride waveguides to the Ge absorbing region [21], [22], and recently a high-speed Ge photodetector integrated with Si_3N_4 waveguide is reported using an evanescent coupling approach [23]. As pointed out by [24], for optical detection, Ge absorbing waveguide layers can be made relatively-large to accommodate the evanescent coupling from Si_3N_4 because it is not necessary to maintain the fundamental mode inside the absorbing layers. On the other hand, for waveguide optical modulator in which light from the modulator's output needed to be coupled back into the photonic circuits, it is necessary to maintain the fundamental mode within the modulator and at the output waveguide. Therefore, the core dimensions of optical modulators would be relatively small and the optical coupling with both input and output waveguides needed to be considered as investigated in the optical integration between Si ($n \sim 3.5$) or SiGe ($n \sim 4$) waveguides and Ge-based ($n \sim 4.3$) optical modulators theoretically [25], [26], [27] and experimentally [28], [29]. As a result, for the optical integration between Si_3N_4 and Ge-based waveguide optical modulators, lateral coupling scheme via amorphous Ge_xSi materials was proposed to facilitate the optical coupling [24], [30]. From the studies, 83% optical transmission (0.8 dB coupling loss) was projected from 3D FDTD calculations, which could be attributed to the absorption in the Ge_xSi amorphous materials, together with the reflection and scattering losses at the butt-coupling interfaces between Ge_xSi amorphous tapers and Ge-based devices. Nevertheless, to further improve the optical coupling performance to be as competitive as that obtainable with the optical integration between SOI waveguides and Ge-based optical modulators [31], a new optical integration scheme is required for the optical integration between Si_3N_4 and Ge-based waveguide optical modulators in order to minimize the coupling loss which is crucial for low-energy optical interconnects.

In this paper, we investigate the optical integration between Si_3N_4 and Ge-based waveguides via vertical coupling configuration for Si_3N_4 waveguide-integrated optical modulators. To vertically and robustly transfer the optical mode from Si_3N_4 to Ge-based devices, amorphous Si (α-Si) is employed as an optical bridge because the optical absorption of α-Si can be expectedly neglected around the operating wavelength of the Ge-based optical modulator of 1.55 μm [32]. Moreover, reflection and scattering losses between different material interfaces could be avoided, and coupling performance of more than 90% optical transmission (<0.46 dB coupling loss) can be obtained. Regarding the robustness of the optical coupling configuration, tolerant analysis with respect to the variation in optical wavelengths and critical parameters of the coupling structure shows that the coupling performance could be promisingly maintained considering fabrication variation in advanced CMOS processes. Finally, we found that the studied coupling structure could be employed to enable a compact Si_3N_4 waveguide-integrated Ge-based optical modulator with a viable extinction ratio and insertion loss performance. In the 3D Finite-Difference-Time-Domain (3D-FDTD) simulations (Ansys-Lumerical), the smallest grid size is $\sim$ 2 nm, and a perfectly matched layer (PML) is employed to suppress reflections from the simulation region boundaries.

II. OPTICAL COUPLING CONFIGURATIONS UNDER INVESTIGATION

Fig. 1(a) shows the schematic views of the investigated optical integration between Si_3N_4 and Ge-based waveguides via vertical coupling configuration. α-Si is employed as an optical bridge to vertically and robustly transfer the optical mode from Si_3N_4 to the Ge-based part. The cladding of the structure is SiO_2 ($n \sim 1.45$). The optical absorption of α-Si can be expectedly neglected around the telecommunication wavelength of 1.55 μm with a compromising refractive index value of $n \sim 3.5$ [32] between that of Si_3N_4 and Ge-based parts; moreover, α-Si has an additional advantage of the ability to be deposited on SiO_2. As depicted in Fig. 1(a-c), two tapering sections are included to transfer the optical mode from Si_3N_4 to α-Si, and from α-Si to the Ge-based part respectively. For potential simplicity of the structure, in this study we decide to investigate the possibility to employ only one linear taper in each of the tapering sections. Therefore, only the α-Si waveguide will be linearly tapered for the optical coupling from Si_3N_4 to α-Si, while for the optical coupling from α-Si to Ge-based part, only the Ge-based part will be linearly tapered. To thoroughly evaluate the optical coupling performance of the structure, we consider several parameters including α-Si thickness (t_1), vertical gap between Si_3N_4 and α-Si (g_1), vertical gap between α-Si and GeSi (g_2), α-Si taper tip width (w_{tSi}), GeSi taper tip width (w_{tGe}), height of Si under Ge-based waveguide (h_{Si}), length of Si_3N_4 slope (L_1), α-Si taper length (L_2), and GeSi taper length (L_3). A number of choices is initially made in this study as follows: (1) the width and thickness values of Si_3N_4 are chosen to be 2 μm and 1 μm, respectively, which are consistent with achievable dimensions of reported low stress Si_3N_4 films using low deposition temperature [13]. The Ge-rich GeSi layer is 600-nm-wide and 200-nm-thick, which is comparable with the previous investigation using lateral coupling configuration [24], [30] and also with some of the Ge-based optical devices reported in literature [25], [26], [28], [29], [31], [33], [34]. It should be noted that light with quasi-transverse-electric (quasi-TE) polarization will be considered in this work as it is typically used in submicron Ge-based waveguide optical modulators [28], [29], [35].

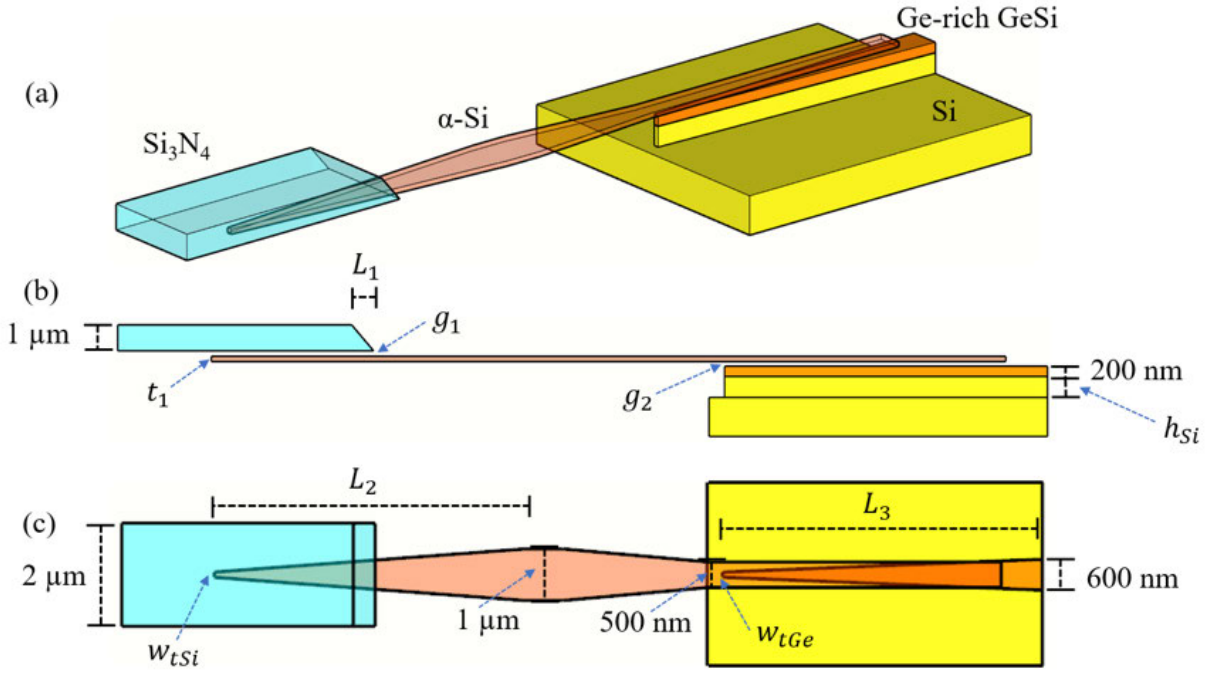

FIGURE 1. (a) Schematic, (b) side, and (c) top views of the investigated the optical integration from Si_3N_4 to Ge-based waveguides via α-Si using vertical coupling configuration. Several parameters are considered during the optimization including α-Si thickness (t_1), vertical gap between Si_3N_4 and α-Si (g_1), vertical gap between α-Si and GeSi (g_2), α-Si taper tip width (w_{tSi}), GeSi taper tip width (w_{tGe}), height of Si under Ge-based waveguide (h_{Si}), length of Si_3N_4 slope (L_1), α-Si taper length (L_2), and GeSi taper length (L_3). The thickness of the Si slab employed in simulation is 1.5 μm. The top and bottom claddings of the α-Si taper and the Si_3N_4 waveguide structures are SiO_2, as Si_3N_4 and α-Si have an additional advantage of the ability to be deposited on SiO_2, which can be reliably deposited on Si. Si Substrate in the region below the α-Si taper structure is not included because the optical mode is well-confined in the guided material layers as in Fig. 2(a).

III. COUPLING PERFORMANCE: RESULTS AND DISCUSSIONS

Fig. 2(a) reports on the optical propagation of the entire investigated coupling scheme from the 2-μm-wide and 1-μm-thick input Si_3N_4 waveguide via the α-Si waveguide vertically to the 600-nm-wide and 200-nm-thick Ge-based layers at the optical wavelength of 1550 nm. After optimization using 3D-FDTD calculations, it can be observed that the quasi-TE fundamental mode at the Si_3N_4 waveguide, indicated in the top left inset, can be adiabatically transferred via the α-Si waveguide to the quasi-TE fundamental mode at the Ge-based layers, indicated in the top right inset, using the vertical coupling configuration. The overall coupling performance from the Si_3N_4 to the Ge-based waveguides of more than 96% optical transmission ($\sim$0.18 dB coupling loss) is observed, which can be attributed to the mode size and effective index mismatch between different waveguides and materials in the coupling scheme. For the first optical coupling section from the Si_3N_4 waveguide to the α-Si part, as indicated in Fig. 2(a), we have arrived at the α-Si linear taper length, L_2, of 45 μm with an α-Si taper tip width, w_{tSi}, of 100 nm while the taper end width is fixed at 1 μm. The thickness of α-Si, t_1, and the vertical gap between Si_3N_4 and α-Si, g_1, are 100 nm and 50 nm, respectively. Fig. 2(b) shows that by linearly widening the width of α-Si waveguide the effective index of the quasi-TE fundamental mode can be smoothly transferred from the Si_3N_4 waveguide to the α-Si one, which is consistent with the phase matching condition of the eigenmodes of a coupled structure described by the supermode theory [36], [37], [38].

The electric field distributions of the optical modes with effective index values at the α-Si taper width values of 0.1, 0.5, and 1 μm can be seen in the Fig. 2(d-f); their corresponding positions along the propagation direction are also indicated by the black arrows. It is important to mention that to avoid an abrupt change in the refractive index value, a slope etching is required at the end of 1-μm-thick Si_3N_4 waveguide as shown in Fig. 1(a-b). The length of this Si_3N_4 slope, L_1, is 4 μm as indicated in Fig. 2(a). Based on the recent advance on the slope etching technique for Si photonics platform [39], we envision that the structure could be obtained, taking into account possible fabrication variations to be later discussed. It should be noted that although a linear width-tapered Si_3N_4 waveguide could provide similar performance, the taper tip width of $\sim$100 nm would be required, so a tradeoff between the realization of slope etching and the requirement to have another structure with $\sim$ 100 nm tip width needs to be weighted. As shown in Fig. 1(c) and also indicated in Fig. 2(a), the α-Si width of 1 μm at the end of α-Si taper will be linearly reduced through a 30-μm-long taper to a α-Si width of 500 nm at the beginning of the second coupling section with the Ge-based waveguide in order to reduce the optical mode size as in Fig. 2(g)

compared to Fig. 2(f), making it more comparable to that of the Ge-based waveguide. Subsequently, for the second coupling section from the 500-nm-wide α-Si waveguide to the 600-nm-wide and 200-nm-thick Ge-based layers, we have arrived at the GeSi taper length, L_3, of 40 μm with a GeSi taper tip width, w_{tGe}, of 100 nm while the taper end width is fixed at 600 nm. The vertical gap between α-Si and GeSi, g_2, is 50 nm as used in the first coupling section. Fig. 2(c) shows that by linearly widening the width of Ge-based waveguide the effective index of the quasi-TE fundamental mode can be smoothly transferred from the α-Si waveguide to the Ge-based ones. The electric field distributions of the optical modes with effective index values at the Ge-based taper width values of 0.1, and 0.3 μm can be seen in the Fig. 2(h-i); their corresponding positions along the propagation direction are also indicated by the black arrows.

As it is important in Si-based photonics to have a robust design against variations in operating wavelengths and large-scale fabrication [40], Fig. 3 reports the coupling performance of the entire coupling structures from the Si_3N_4 to the Ge-based waveguides with respect to the variations in optical wavelengths within the C-band region from 1530 to 1565 nm, α-Si thickness (t_1), vertical gap between Si_3N_4 and α-Si (g_1), vertical gap between α-Si and GeSi (g_2), α-Si taper tip width (w_{tSi}), GeSi taper tip width (w_{tGe}), height of Si under Ge-based waveguide (h_{Si}), and Si_3N_4 slope length (L_1). It is important to note that from the obtained optical propagation, the α-Si taper length (L_2) and the GeSi taper length (L_3) can be considered not critical in our design because the optical modes have been successfully transferred into the α-Si and GeSi regions before the end of the taper for both the first and second coupling sections as in Fig. 2(a); therefore, large variation in the L_2 and L_3 values can be tolerated, which will be considered in the next section when the insertion loss of an integrated optical modulator has to be taken into account. Fig. 3(a) shows that the aforementioned optimized coupling performance of ~0.18 dB loss can be maintained over the entire C-band wavelength region, which is the typical operating range of Ge-based optical devices [41]. The effects of variation in α-Si thickness (t_1), vertical gap between Si_3N_4 and α-Si (g_1), and vertical gap between α-Si and GeSi (g_2) are also considered in Fig. 3(b-d), respectively. For t_1, the coupling performance will not be significantly deviated from the optimized value as long as the thickness variation is within $\pm$10 nm from the designed value of 100 nm as in Fig. 3(b). For g_1 and g_2, the coupling performance is found to be relatively unaffected as long as the thickness variation is within $\pm$20 nm from the designed value of 50 nm as in Fig. 3(c-d). As the refractive index of α-Si is much higher than SiO_2, the variation in α-Si thickness (t_1) would expectedly affects the coupling performance more than the variations in vertical gap between Si_3N_4 and α-Si (g_1) and vertical gap between α-Si and GeSi (g_2) which are made of SiO_2. Although challenging, these variations can be considered within the homogenous performance recently obtained from advanced CMOS process technology for sub-wavelength photonic structures on a Si wafer [14], [42], [43], [44]. The effects of variation in α-Si taper tip width (w_{tSi}), and GeSi taper tip width (w_{tGe}) are also considered in Fig. 3(e-f). Considering the varied resolution of different lithography technologies and obtainable etching aspect ratio in Si platform, we focus on investigating the coupling performance when the values of w_{tSi} and w_{tGe} have been wider than the design value of 100 nm. For w_{tSi}, the coupling performance is found to be relatively unaffected even with +40 nm deviation (w_{tSi} = 140 nm) as in Fig. 3(e). For w_{tGe}, the coupling performance will slightly deviate from the optimized value with +20 nm deviation (w_{tGe} = 120 nm); nevertheless, optical coupling loss as low as ~0.27 dB can be maintained even with +40 nm deviation (w_{tGe} = 140 nm). To explicate, consistent with the above findings in the cases of t_1, g_1, and g_2, the deviation in w_{tGe} affects the coupling performance slightly more than the deviation in w_{tSi} mainly because the refractive index of Ge-based layers is more than that of α-Si; therefore, the effective index of the former will be more sensitive to the slight changes in waveguide dimension than that of the latter. For the height of Si under Ge-based waveguide (h_{Si}), Fig. 3(g) shows that h_{Si} of at least 1.2 μm is required in order to achieve optimized coupling performance of ~0.18 dB loss. Promisingly, it should be noted that with the advance in Si technologies, high aspect ratio etching of more than 35 (1500/40 nm) can be obtained in Si platform [45], [46]. The aspect ratio of ~10-15 {(h_{Si}+200)/ w_{tGe}} at the beginning of GeSi taper region should be considered obtainable on Si platform. Notably, it should be mentioned that the optical coupling scheme could also be applicable to the Ge/SiGe multiple quantum wells (MQWs). Although, care should be taken as the state-of-the-art progress showed that a Ge-rich SiGe relaxed buffer of more than 200 nm is still required to grow high quality Ge/SiGe MQWs on Si [26] leading to a total Ge-rich SiGe thickness of more than 500 nm, which would result in a slight increase in the required aspect ratio (~17) at the beginning of GeSi taper region. Finally, the slight variation in the slope angle resulting in varied Si_3N_4 slope length, L_1, can be also expected. As in Fig. 3(h), the optimized coupling performance of ~0.18 dB loss can be maintained as long as $L_1 \geq 4$ μm and the optical coupling loss as low as ~0.27 dB can be maintained with L_1 of 3 μm; therefore, the variation in L_1 can be tolerated.

IV. INTEGRATED OPTICAL MODULATION PERFORMANCE

To investigate the potential usage of the coupling structure, Si_3N_4 waveguide-integrated Ge-based optical modulators are studied using the obtained coupling scheme as in Fig. 4(a) showing the integration of a Ge-based optical modulator with Si_3N_4 input and output waveguides. To be able to apply an electrical bias on the GeSi region, we assume a vertical p-i-n junction. The Si under the Ge-rich GeSi part is assumed to be p-type, and the top 30 nm of the Ge-rich GeSi part is assumed to be n-type with a doping concentration of ~5×10^{18} cm^{-3}. Notably, it was experimentally shown that

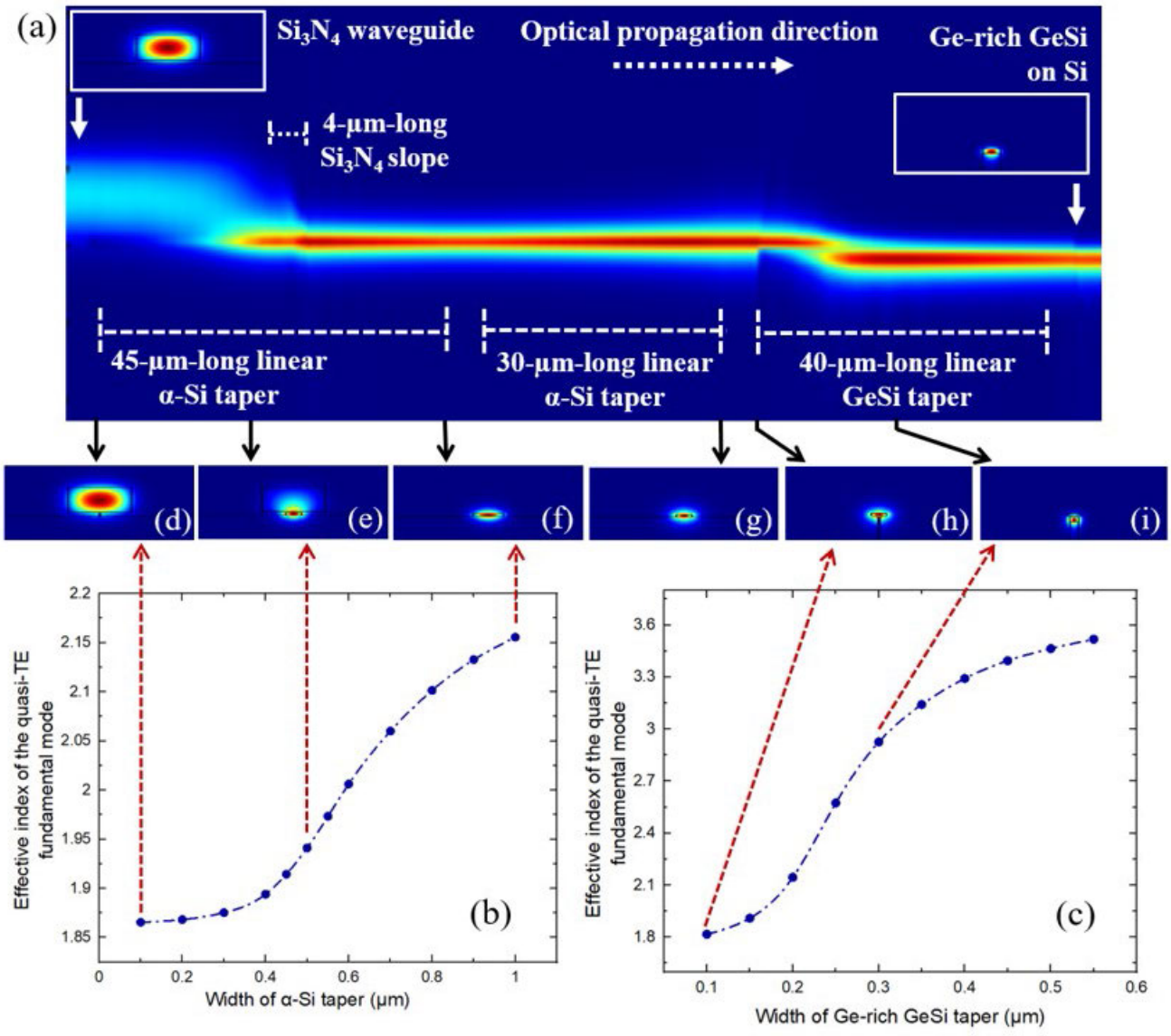

FIGURE 2. (a) Optical propagation of the entire coupling structure from the 2-μm-wide and 1-μm-thick input Si_3N_4 waveguide via the α-Si waveguide vertically to the 600-nm-wide and 200-nm-thick Ge-based waveguide at the optical wavelength of 1550 nm. (b) Effective index of the quasi-TE fundamental mode which can be transferred from the Si_3N_4 waveguide to the α-Si one by linearly widening the width of α-Si taper. (c) Effective index of the quasi-TE fundamental mode which can be transferred from the α-Si waveguide to the Ge-based one by linearly widening the width of Ge-based part. Electric field distributions of the optical modes (d-f) at the α-Si taper width values of 0.1, 0.5, and 1 μm, (g) in α-Si before entering the second coupling section, (h-i) at the GeSi taper width values of 0.1, and 0.3 μm. The corresponding positions along the propagation direction are indicated by the black arrows.

electrical bias could be effectively applied across a Ge-based vertical p-i-n junction using a relatively-thin n-type layer of 10 nm [47].

Contrary to the previous section focusing on the optical coupling loss mainly due to the mode size and effective index mismatch and hence only the real part of refractive index (n) of Ge-based material is included in the simulation, the imaginary part of refractive index (k) has to be included also in this section in order to properly evaluate the insertion loss of the integrated optical modulator. The absorption data of the Ge-rich GeSi material were as reported from $Ge_{0.9925}Si_{0.0075}$ in [25] for Franz-Keldysh effect (FKE) modulator at the optical wavelength of 1.55 μm.

To be comparable to the previous related works [24], [31], the absorption changes due to the FKE, which is intrinsically fast [48], between the electric field of ~10 kV/cm ($\alpha \sim 150$ cm^{-1}, taking into account the Ge indirect-gap absorption) for the on-state operation, and ~95 kV/cm ($\alpha \sim 650$ cm^{-1}) for the off-state operation in the 170-nm-thick Ge-rich GeSi layer are employed as indicate in Fig. 4(b-c). This also ensures that the driving voltage would be less than 2 V drivable voltage of CMOS [49], [50], [51], and the electric field would not be higher than the breakdown field of the bulk

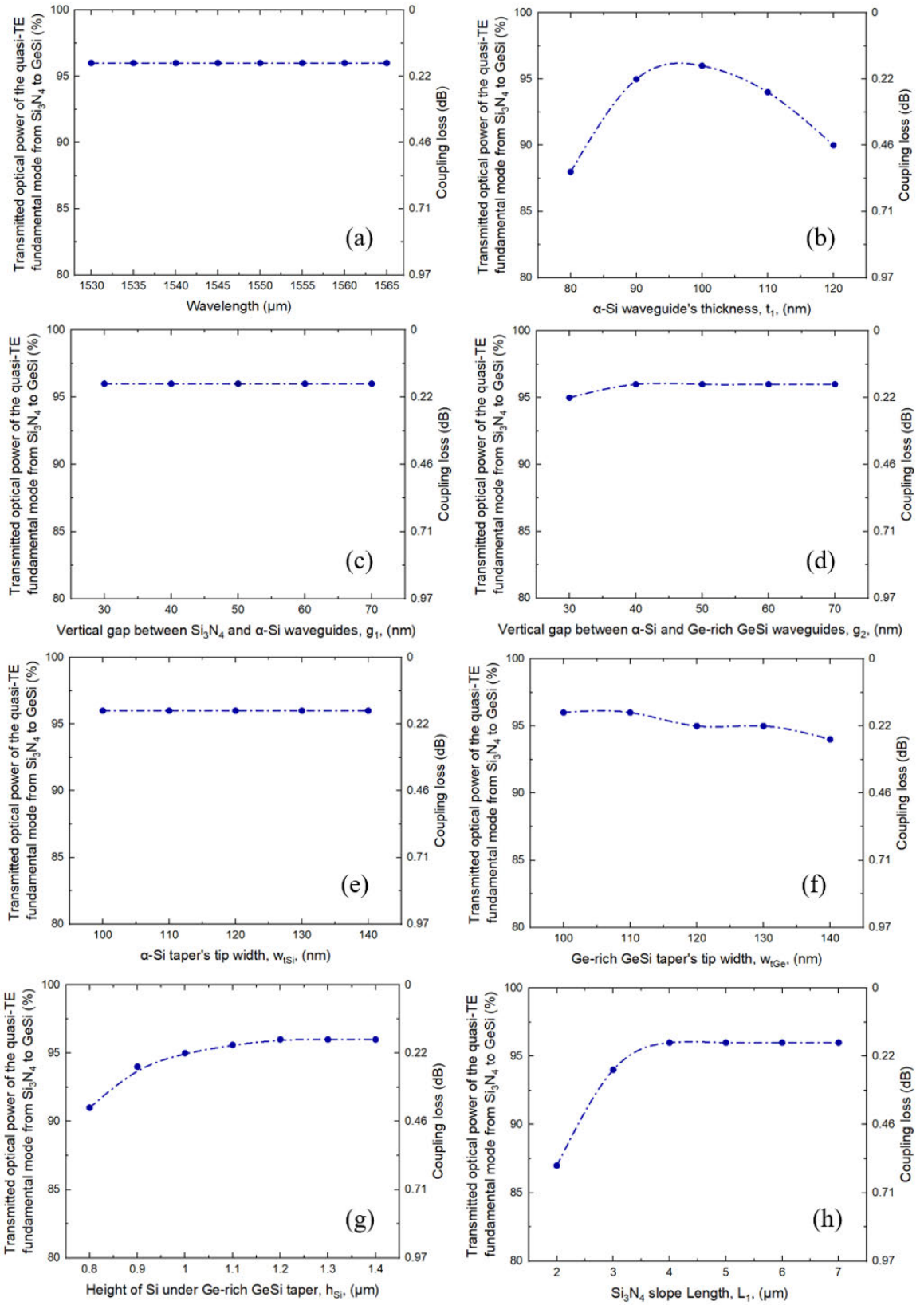

FIGURE 3. The coupling performance of the entire coupling structures from the Si_3N_4 to the Ge-based waveguides with respect to the variations in (a) optical wavelengths within the C-band region, (b) α-Si thickness, t_1, (c) vertical gap between Si_3N_4 and α-Si, g_1, (d) vertical gap between α-Si and GeSi, g_2, (e) α-Si taper tip width, w_{tSi}, (f) GeSi taper tip width, w_{tGe}, (g) height of Si under Ge-based waveguide, h_{Si}, and (h) Si_3N_4 slope length, L_1.

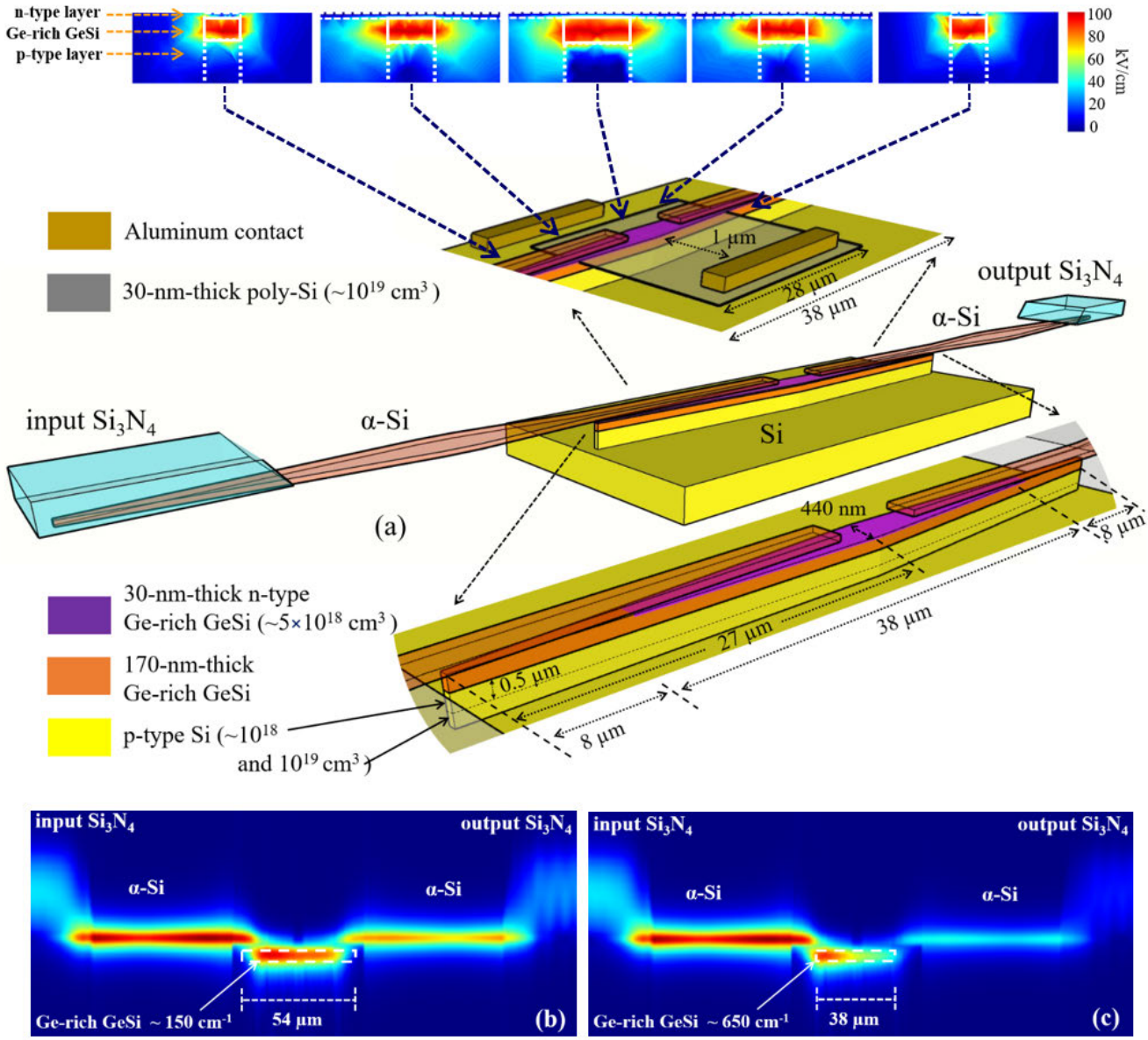

FIGURE 4. (a) The integration of a Ge-based optical modulator with Si_3N_4 input and output waveguides; the top inset indicates the top and bottom metal contacts, that are put laterally away from the vertical p-i-n junction. The optical propagation of Si_3N_4 waveguide-integrated Ge-based optical modulators from the Si_3N_4 input to the Si_3N_4 output waveguides based on the obtained coupling scheme for (b) the on-state operation and (c) the off-state operation. The optical mode can propagate from the input Si_3N_4 waveguide to the output Si_3N_4 waveguide effectively. The top insets show electric field distribution cross sections at different positions along the 38-μm-long Ge-rich GeSi region. The electric field can be effectively applied along the active region via the 28-μm-long laterally-extending n-type poly-Si layer.

Ge material ~100 kV/cm [52]. The free carrier absorption data in the p- and n-layers with a doping concentration of $\sim 1 \times 10^{18}$ and $\sim 5 \times 10^{18}$ cm^{-3} were calculated using the Drude model [53], [54]. Significantly, in order to have a low-loss optical modulator during the on-state operation, the GeSi taper length (L_3) of 27 μm is used instead of 40 μm, taking advantage of the fact that the optical mode has been successfully transferred into the GeSi regions before the end of the GeSi taper, as previously discussed in the section III. As a result, the end of the Ge-rich GeSi taper would be 440-nm-wide. Additionally, it should be noted that during the off-state operation the electrical field does not need to be applied in the first 8 μm part of both Ge-rich GeSi tapers because the optical mode is not yet coupled into this Ge-rich GeSi section as previously shown in Fig. 2(a); therefore, the total length of the Ge-rich GeSi region with $\alpha \sim 650$ cm^{-1} would be 38 μm as indicated in Fig. 4(a) and (c), and to be conservative $\alpha \sim 150$ cm^{-1} of the on-state operation will be maintained in the first 8 μm part of both Ge-rich GeSi tapers. As also discussed in [30], [55], the fact that the narrow parts of tapers can be excluded from the modulation section, i.e. by proton implantation to decrease the n-doping, is significant because it helps prevent the overall capacitance values of the device from increasing due to the very narrow

structure around the tip part of tapers. Regarding the top and bottom metal contact metallization, we envision that they can be put laterally away from the vertical p-i-n junction to minimize the optical loss due to metal [28]. As in the top inset of Fig. 4(a), based on the previous works [56], a lateral n-type poly-Si layer could be assumed to allow a top contact metallization; an n-doping concentration of 10^{19} cm^{-3} is preferred in order to have resistivity of as low as $\sim 5 \times 10^{-3}\Omega$·m [57] and allow a low resistance using 30-nm-thick poly-Si layer. It should be noted that $10^{19} - 10^{20}$ n-type phosphorous doping concentration was experimentally obtained in poly-Si layer using implantation technique with a relative low activation annealing temperature in Ge-based p-i-n structure [56]. Similarly, to ensure a sufficiently low resistivity of $\sim 3 \times 10^{-3}\Omega$·m [58], [59] for the n-doped Ge-rich GeSi, 5×10^{18} cm^{-3} is assumed. To avoid extra losses caused by electrodes, they are put at least 1 μm away from the waveguide active region. It is important to note that although the top contact metallization is placed only on one side of the structure, on the other side the poly-Si layer needs to be deposited laterally for at least 1 μm as well in order to optically maintain the structure symmetry ensuring a low-loss propagation. The top insets of Fig. 4(a) show electric field distribution cross sections at different positions along the 38-μm-long Ge-rich GeSi region. The electric field can be effectively applied along the active region via the 28-μm-long laterally-extending n-type poly-Si layer. The electric field is relatively uniform across the active region using CMOS drivable voltage of less than 2 V. The refractive index of thin poly-Si layer at the optical wavelength of 1550 nm is as consistently in [60] and [61], and its free carrier absorption can be estimated as in [56]. For the first 0.5 μm of the p-type Si layer under the Ge-rich GeSi, a p-doping concentration of 10^{18} cm^{-3} is enough to allow a sufficiently-low resistivity of $\sim 5 \times 10^{-2}\Omega$·m [62], while the p-doping concentration of the remaining p-type part leading to the bottom electrode can be increased to 10^{19} cm^{-3}, allowing low resistivity of $\sim 8 \times 10^{-3}\Omega$·m [62] without significant contribution toward the optical loss. As the field-induced absorption change due to electroabsorption (EA) such as the Franz-Keldysh effect is intrinsically fast [63], [64], [65], the 3-dB bandwidth of the modulator could be reasonably expected to be limited by the RC time constant [28], [31]. Based on the resistivity information of different layers given above, the series resistance R can be conservatively estimated to be 100 Ω, while the capacitance C of the 38-μm-long active region can be calculated to be $\sim$ 10 fF. As a result, taking into account an external load resistance of 50 Ω, the 3-dB bandwidth can theoretically reach $\sim$ 100 GHz. Regarding the energy consumption per bit, which could be estimated by energy/bit $= 1/2(CV^2)$ [31], [66], 20 fJ/bit is obtained with a driving voltage between 0 and 2 V, which is comparable to that obtainable with the state-of-the-art devices [15]. Additionally, it should be noted that Aluminum (Al) contact can be assumed, and high-speed operations have been shown by using Al contact in GeSi-based optical devices [67], [68].

As in Fig. 4(b-c) based on the obtained coupling scheme, the fundamental quasi-TE mode can propagate from the input Si_3N_4 waveguide to the output Si_3N_4 waveguide effectively for both on-state and off-state operations. From 3D-FDTD calculations, the Si_3N_4 waveguide-integrated Ge-based optical modulator exhibits extinction ratio (ER), i.e. the ratio between the optical power at the output Si_3N_4 waveguide at the on-state and off-state operations: $10\log_{10}(I_{out,\ on-state}/I_{out,off-state})$, of $\sim$ 10.7 dB, and the insertion loss (IL), i.e. the ratio between the optical power at the input Si_3N_4 waveguide and that at the output Si_3N_4 waveguide during the on-state operation: $10\log_{10}(I_{in}/I_{out,\ on-state})$, of $\sim$ 5.2 dB, which includes the coupling loss between the Si_3N_4 input (resp. output) waveguide and Ge-based layers through α-Si due to the mode size and effective index mismatch, the optical absorption due to the p- and n-layers, and the optical absorption in the Ge-rich GeSi layer during the on-state operation. The integrated performance of 10.7-dB ER obtained simultaneously with 5.2-dB IL (ER/IL > 2) significantly improves from the previous projected ER/IL of $\sim$ 1 obtained with a lateral coupling scheme [24]. Moreover, the results indicate that with the addition of α-Si layers it is possible to obtain a Si_3N_4 waveguide-integrated Ge-based optical modulator with comparable ER/IL performance to one of the recently reported Ge-based optical modulators integrated with SOI waveguide platform optimized via 3D-FDTD analysis [31], increasing the promise of Si_3N_4-based photonic integrated circuits. Lastly, the analysis of using α-Si as an optical bridge for vertical integration between Si_3N_4 and Ge-rich GeSi structure presented in this work could provide an additional basis for further usage in related on-going research efforts such as multi-layer photonic integrated circuits for three dimensional (3D) optical integration [8], [39], [69], [70] with a view to including a higher refractive index material such as Ge into the platform.

V. CONCLUSION

Si_3N_4 photonic integrated circuits have gain significant and rapid interest in different photonic applications thanks to its superior passive performance in terms of loss, bandwidth, and high power-handling capability comparing to the SOI platform. Nevertheless, optical integration between Si_3N_4 and Ge-based optical components that can be as efficient as that obtainable with the SOI platform remains critically challenging especially for optical modulation. In this paper, via 3D-FDTD calculations we investigate the optical integration between Si_3N_4 and Ge-based waveguides via vertical coupling configuration employing α-Si as an optical bridge showing coupling efficiency of more than 90%. The tolerant analysis with respect to variations in optical wavelengths and critical parameters of the coupling structure shows that the coupling performance could be maintained considering fabrication variation in advanced CMOS processes. Last but not least, we found that the studied coupling structure could be employed to enable a low-voltage Si_3N_4 waveguide-integrated Ge-based optical modulator with an

ER/IL performance (>2) comparable to one of the recently reported Ge-based optical modulators integrated with an SOI waveguide platform optimized via 3D-FDTD analysis, increasing the prospect of Si_3N_4-based photonic integrated circuits for low-energy optical interconnects.

REFERENCES

[1] A. Rahim, E. Ryckeboer, A. Z. Subramanian, S. Clemmen, B. Kuyken, A. Dhakal, A. Raza, A. Hermans, M. Muneeb, S. Dhoore, Y. Li, U. Dave, P. Bienstman, N. Le Thomas, G. Roelkens, D. Van Thourhout, P. Helin, S. Severi, X. Rottenberg, and R. Baets, "Expanding the silicon photonics portfolio with silicon nitride photonic integrated circuits," *J. Lightw. Technol.*, vol. 35, no. 4, pp. 639–649, Feb. 15, 2017.

[2] Z. Zhang, M. Yako, K. Ju, N. Kawai, P. Chaisakul, T. Tsuchizawa, M. Hikita, K. Yamada, Y. Ishikawa, and K. Wada, "A new material platform of Si photonics for implementing architecture of dense wavelength division multiplexing on Si bulk wafer," *Sci. Technol. Adv. Mater.*, vol. 18, no. 1, pp. 283–293, Dec. 2017.

[3] D. J. Blumenthal, R. Heideman, D. Geuzebroek, A. Leinse, and C. Roeloffzen, "Silicon nitride in silicon photonics," *Proc. IEEE*, vol. 106, no. 12, pp. 2209–2231, Dec. 2018.

[4] Q. Wilmart, H. El Dirani, N. Tyler, D. Fowler, S. Malhouitre, S. Garcia, M. Casale, S. Kerdiles, K. Hassan, C. Monat, X. Letartre, A. Kamel, M. Pu, K. Yvind, L. Oxenløwe, W. Rabaud, C. Sciancalepore, B. Szelag, and S. Olivier, "A versatile silicon-silicon nitride photonics platform for enhanced functionalities and applications," *Appl. Sci.*, vol. 9, no. 2, p. 255, Jan. 2019.

[5] Y. Chen, T. D. Bucio, A. Z. Khokhar, M. Banakar, K. Grabska, F. Y. Gardes, R. Halir, I. Molina-Fernandez, P. Cheben, and J.-J. He, "Experimental demonstration of an apodized-imaging chip-fiber grating coupler for Si_3N_4 waveguides," *Opt. Lett.*, vol. 42, no. 18, pp. 3566–3569, 2017.

[6] T. D. Bucio, C. Lacava, M. Clementi, J. Faneca, I. Skandalos, M. Galli, K. Debnath, A. Baldycheva, P. Petropoulos, and F. Gardes, "Silicon nitride photonics for the near-infrared," *IEEE J. Sel. Top. Quantum Electron.*, vol. 26, no. 2, pp. 1–13, Mar./Apr. 2020.

[7] C. Xiang, W. Jin, and J. E. Bowers, "Silicon nitride passive and active photonic integrated circuits: Trends and prospects," *Photon. Res.*, vol. 10, no. 6, p. A82, Jun. 2022.

[8] K. Shang, S. Pathak, B. Guan, G. Liu, and S. J. B. Yoo, "Low-loss compact multilayer silicon nitride platform for 3D photonic integrated circuits," *Opt. Exp.*, vol. 23, no. 16, pp. 21334–21342, 2015.

[9] F. J. Bauters, J. R. M. Heck, D. John, D. Dai, M.-C. Tien, S. J. Barton, A. Leinse, G. R. Heideman, J. D. Blumenthal, and E. J. Bowers, "Ultra-low-loss high-aspect-ratio Si_3N_4 waveguides," *Opt. Exp.*, vol. 19, no. 4, pp. 3163–3174, 2011.

[10] S. Cheung and M. R. Tan, "Ultra-low loss and fabrication tolerant silicon nitride (Si_3N_4)(de-) muxes for 1-μm CWDM optical interconnects," in *Proc. Opt. Fiber Commun. Conf.*, 2020, paper M3F.6 doi: 10.1364/OFC.2020.M3F.6.

[11] H. El Dirani, M. Casale, S. Kerdiles, C. Socquet-Clerc, X. Letartre, C. Monat, and C. Sciancalepore, "Crack-free silicon-nitride-on-insulator nonlinear circuits for continuum generation in the C-band," *IEEE Photon. Technol. Lett.*, vol. 30, no. 4, pp. 355–358, Feb. 15, 2018.

[12] K. Luke, A. Dutt, C. B. Poitras, and M. Lipson, "Overcoming Si_3N_4 film stress limitations for high quality factor ring resonators," *Opt. Exp.* vol. 21, no. 19, pp. 22829–22833, 2013.

[13] X. Cheng, J. Hong, A. M. Spring, and S. Yokoyama, "Fabrication of a high-Q factor ring resonator using LSCVD deposited Si_3N_4 film," *Opt. Mater. Exp.* vol. 7, no. 7, pp. 2182–2187, 2017.

[14] M. H. P. Pfeiffer, C. Herkommer, J. Liu, T. Morais, M. Zervas, M. Geiselmann, and T. J. Kippenberg, "Photonic Damascene process for low-loss, high-confinement silicon nitride waveguides," *IEEE J. Sel. Topics Quantum Electron.*, vol. 24, no. 4, Jul. 2018, Art. no. 6101411.

[15] X. Wang and J. Liu, "Emerging technologies in Si active photonics," *J. Semicond.*, vol. 39, no. 6, Jun. 2018, Art. no. 061001.

[16] K. Wada and L. C. Kimerling, *Photonics and Electronics With Germanium*. Weinheim, Germany: Wiley, 2015.

[17] D. Marris-Morini, V. Vakarin, J. M. Ramirez, Q. Liu, A. Ballabio, J. Frigerio, M. Montesinos, C. Alonso-Ramos, X. Le Roux, S. Serna, D. Benedikovic, D. Chrastina, L. Vivien, and G. Isella, "Germanium-based integrated photonics from near- to mid-infrared applications," *Nanophotonics*, vol. 7, no. 11, pp. 1781–1793, 2018.

[18] D. Feng, W. Qian, H. Liang, C.-C. Kung, Z. Zhou, Z. Li, J. S. Levy, R. Shafiiha, J. Fong, B. J. Luff, and M. Asghari, "High-speed GeSi electroabsorption modulator on the SOI waveguide platform," *IEEE J. Sel. Topics Quantum Electron.*, vol. 19, no. 6, pp. 64–73, Nov. 2013.

[19] J. Liu, "Monolithically integrated Ge-on-Si active photonics," *Photonics*, vol. 1, no. 3, pp. 162–197, Jul. 2014.

[20] L. Chen, C. R. Doerr, L. Buhl, Y. Baeyens, and R. A. Aroca, "Monolithically integrated 40-wavelength demultiplexer and photodetector array on silicon," *IEEE Photon. Technol. Lett.*, vol. 23, no. 13, pp. 869–871, Jul. 2011.

[21] D. Ahn, C.-Y. Hong, J. Liu, W. Giziewicz, M. Beals, L. C. Kimerling, J. Michel, J. Chen, and F. X. Kartner, "High performance, waveguide integrated Ge photodetectors," *Opt. Exp.*, vol. 15, no. 7, pp. 3916–3921, 2007.

[22] D. Ahn, L. C. Kimerling, and J. Michel, "Efficient evanescent wave coupling conditions for waveguide-integrated thin-film Si/Ge photodetectors on silicon-on-insulator/germanium-on-insulator substrates," *J. Appl. Phys.*, vol. 110, no. 8, Oct. 2011, Art. no. 083115.

[23] X. Hu, D. Wu, D. Chen, L. Wang, X. Xiao, and S. Yu, "180 Gbit/s Si_3N_4-waveguide coupled germanium photodetector with improved quantum efficiency," *Opt. Lett.*, vol. 46, no. 24, pp. 6019–6022, 2021.

[24] W. Traiwattanapong, K. Wada, and P. Chaisakul, "Analysis of optical integration between Si_3N_4 waveguide and a Ge-based optical modulator using a lateral amorphous GeSi taper at the telecommunication wavelength of 1.55 μm," *Appl. Sci.*, vol. 9, no. 18, p. 3846, Sep. 2019.

[25] J. Liu, D. Pan, S. Jongthammanurak, K. Wada, L. C. Kimerling, and J. Michel, "Design of monolithically integrated GeSi electro-absorption modulators and photodetectors on an SOI platform," *Opt. Exp.*, vol. 15, no. 2, pp. 623–628, 2007.

[26] E. H. Edwards, L. Lever, E. T. Fei, T. I. Kamins, Z. Ikonic, J. S. Harris, R. W. Kelsall, and D. A. B. Miller, "Low-voltage broad-band electroabsorption from thin Ge/SiGe quantum wells epitaxially grown on silicon," *Opt. Exp.*, vol. 21, pp. 867–876, Jan. 2013.

[27] W. Traiwattanapong, P. Chaisakul, J. Frigerio, D. Chrastina, G. Isella, L. Vivien, and D. Marris-Morini, "Design and simulation of waveguide-integrated Ge/SiGe quantum-confined stark effect optical modulator based on adiabatic coupling with SiGe waveguide," *AIP Adv.*, vol. 11, no. 3, Mar. 2021, Art. no. 035117.

[28] J. Liu, M. Beals, A. Pomerene, S. Bernardis, R. Sun, J. Cheng, L. C. Kimerling, and J. Michel, "Waveguide-integrated, ultralow-energy GeSi electro-absorption modulators," *Nature Photon.*, vol. 2, pp. 433–437, Jul. 2008.

[29] S. A. Srinivasan, M. Pantouvaki, S. Gupta, H. T. Chen, P. Verheyen, G. Lepage, G. Roelkens, K. Saraswat, D. Van Thourhout, P. Absil, and J. Van Campenhout, "56Gb/s germanium waveguide electro-absorption modulator," *J. Lightw. Technol.*, vol. 34, no. 2, pp. 419–424, 2016.

[30] W. Traiwattanapong, K. Wada, and P. Chaisakul, "FDTD investigation on compact and wideband optical integration between Si_3N_4 and Ge-based waveguide devices via amorphous Si and GeSi lateral tapers," *Results Phys.*, vol. 18, Sep. 2020, Art. no. 103256.

[31] L. Wu, Y. Zhou, Y. Cai, X. Cao, R. Wang, M. Qi, J. Fong, D. Feng, and A. Wu, "Design of a broadband $Ge_{1-x}Si_x$ electro-absorption modulator based on the Franz–Keldysh effect with thermal tuning," *Opt. Exp.*, vol. 28, no. 5, pp. 7585–7595, 2020.

[32] D. T. Pierce and W. E. Spicer, "Electronic structure of amorphous Si from photoemission and optical studies," *Phys. Rev. B, Condens. Matter*, vol. 5, no. 8, pp. 3017–3029, Apr. 1972.

[33] H. Chen, P. Verheyen, P. De Heyn, G. Lepage, J. De Coster, S. Balakrishnan, P. Absil, W. Yao, L. Shen, G. Roelkens, and J. Van Campenhout, "−1 V bias 67 GHz bandwidth Si-contacted germanium waveguide p-i-n photodetector for optical links at 56 Gbps and beyond," *Opt. Exp.*, vol. 24, no. 5, pp. 4622–4631, 2016.

[34] J. Fujikata, M. Noguchi, K. Kawashita, R. Katamawari, S. Takahashi, M. Nishimura, H. Ono, D. Shimura, H. Takahashi, H. Yaegashi, T. Nakamura, and Y. Ishikawa, "High-speed Ge/Si electro-absorption optical modulator in C-band operation wavelengths," *Opt. Exp.*, vol. 28, no. 22, pp. 33123–33134, Oct. 2020.

[35] L. Mastronardi, M. Banakar, A. Z. Khokhar, N. Hattasan, T. Rutirawut, T. D. Bucio, K. M. Grabska, C. Littlejohns, A. Bazin, G. Mashanovich, and F. Y. Gardes, "High-speed Si/GeSi hetero-structure electro absorption modulator," *Opt. Exp.*, vol. 26, no. 6, pp. 6663–6673, Mar. 2018.

[36] H. Duprez, "From design to characterization of hybrid III-V on silicon lasers for photonic integrated circuits," Ph.D. thesis, Institut des Nanotechnologies de Lyon (INL), Univ. de Lyon, Lyon, France, 2016.

[37] H. Duprez, A. Descos, T. Ferrotti, C. Sciancalepore, C. Jany, K. Hassan, C. Seassal, S. Menezo, and B. B. Bakir, "1310 nm hybrid InP/InGaAsP on silicon distributed feedback laser with high side-mode suppression ratio," *Opt. Exp.*, vol. 23, no. 7, pp. 8489–8497, 2015.

[38] A. Yariv and X. Sun, "Supermode Si/III-V hybrid lasers, optical amplifiers and modulators: A proposal and analysis," *Opt. Exp.*, vol. 15, no. 15, pp. 9147–9151, 2007.

[39] R. Petra, S. Z. Oo, A. Tarazona, R. Cernansky, S. A. Reynolds, A. Z. Khokhar, V. Mittal, D. J. Thomson, A. Politi, G. Z. Mashanovich, G. T. Reed, and H. M. H. Chong, "HWCVD a-Si: H interlayer slope waveguide coupler for multilayer silicon photonics platform," *Opt. Exp.*, vol. 27, no. 11, pp. 15735–15749, 2019.

[40] G. Chang, "Wonderland of silicon photonics: An interview with professor Michal Lipson," *Adv. Photon.*, vol. 3, no. 3, Jun. 2021, Art. no. 030501.

[41] L. M. Nguyen, R. Kuroyanagi, T. Tsuchizawa, Y. Ishikawa, K. Yamada, and K. Wada, "Stress tuning of the fundamental absorption edge of pure germanium waveguides," *Opt. Exp.*, vol. 23, no. 14, pp. 18487–18492, 2015.

[42] S. K. Selvaraja, P. De Heyn, G. Winroth, P. Ong, G. Lepage, C. Cailler, A. Rigny, K. K. Bourdelle, W. Bogaerts, D. Van Thourhout, J. Van Campenhout, and P. Absil, "Highly uniform and low-loss passive silicon photonics devices using a 300 mm CMOS platform," in *Proc. Opt. Fiber Commun. Conf.*, 2014, p. 33.

[43] T. Horikawa, D. Shimura, H. Okayama, S.-H. Jeong, H. Takahashi, J. Ushida, Y. Sobu, A. Shiina, M. Tokushima, K. Kinoshita, and T. Mogami, "A 300-mm silicon photonics platform for large-scale device integration," *IEEE J. Sel. Topics Quantum Electron.*, vol. 24, no. 4, Jul. 2018, Art. no. 8200415.

[44] N. B. Feilchenfeld, K. Nummy, T. Barwicz, D. Gill, E. Kiewra, R. Leidy, J. S. Orcutt, J. Rosenberg, A. D. Stricker, C. Whiting, and J. Ayala, "Silicon photonics and challenges for fabrication," in *Proc. SPIE*, vol. 10149, Mar. 2017, Art. no. 101490D.

[45] B. Wu, A. Kumar, and S. Pamarthy, "High aspect ratio silicon etch: A review," *J. Appl. Phys.*, vol. 108, no. 5, Sep. 2010, Art. no. 051101.

[46] R. Abdolvand and F. Ayazi, "An advanced reactive ion etching process for very high aspect-ratio sub-micron wide trenches in silicon," *Sens. Actuators A, Phys.*, vol. 144, no. 1, pp. 109–116, May 2008.

[47] P. Chaisakul, D. Marris-Morini, N. Abadía, J. Frigerio, G. Isella, D. Chrastina, S. Olivier, R. E. De Lamaestre, T. Bernardin, J.-C. Weeber, and L. Vivien, "Ge quantum well plasmon-enhanced quantum confined stark effect modulator," *MRS Proc. Library*, vol. 1627, pp. 1–6, Jan. 2014.

[48] A. Frova and P. Handler, "Franz–Keldysh effect in the space-charge region of a germanium *p–n* junction," *Phys. Rev.*, vol. 137, no. 6, pp. 1857–1861, Mar. 1965.

[49] D. Thomson, A. Zilkie, J. E. Bowers, T. Komljenovic, G. T. Reed, L. Vivien, D. Marris-Morini, E. Cassan, L. Virot, J.-M. Fedeli, J.-M. Hartmann, J. H. Schmid, D.-X. Xu, F. Boeuf, P. O'Brien, G. Z. Mashanovich, and M. Nedeljkovic, "Roadmap on silicon photonics," *J. Opt.*, vol. 18, Jun. 2016, Art. no. 073003.

[50] A. V. Krishnamoorthy, X. Zheng, D. Feng, J. Lexau, J. F. Buckwalter, H. D. Thacker, F. Liu, Y. Luo, E. Chang, P. Amberg, and I. Shubin, "A low-power, high-speed, 9-channel germanium-silicon electroabsorption modulator array integrated with digital CMOS driver and wavelength multiplexer," *Opt. Exp.*, vol. 22, no. 10, pp. 12289–12295, 2014.

[51] P. Chaisakul, V. Vakarin, J. Frigerio, D. Chrastina, G. Isella, L. Vivien, and D. Marris-Morini, "Recent progress on Ge/SiGe quantum well optical modulators, detectors, and emitters for optical interconnects," *Photonics*, vol. 6, no. 1, p. 24, Mar. 2019.

[52] A. S. Kyuregyan and S. N. Yurkov, "Room-temperature avalanche breakdown voltages of Si, Ge, SiC, GaAs, GaP and InP," *Sov. Phys. Semicond.*, vol. 23, pp. 1126–1132, Jan. 1989.

[53] M.-S. Rouifed, "Modulateurs à base de puits quantiques Ge/SiGe pour la photonique sur silicium," Ph.D. thesis, Institut d'Électronique Fondamentale, Univ. Paris Sud-Paris XI, Orsay, France, 2014.

[54] M.-S. Rouifed, D. Marris-Morini, P. Chaisakul, J. Frigerio, G. Isella, D. Chrastina, S. Edmond, X. Le Roux, J.-R. Coudevylle, D. Bouville, and L. Vivien, "Advances toward Ge/SiGe quantum-well waveguide modulators at 1.3 μm," *IEEE J. Sel. Topics Quantum Electron.*, vol. 20, no. 4, pp. 33–39, Jul. 2014.

[55] Y. Tang, H. W. Chen, S. Jain, J. D. Peters, U. Westergren, and J. E. Bowers, "50 Gb/s hybrid silicon traveling-wave electroabsorption modulator," *Opt. Exp.*, vol. 19, no. 7, pp. 5811–5816, 2011.

[56] J. Liu, "GeSi photodetectors and electro-absorption modulators for Si electronicphotonic integrated circuits," Ph.D. dissertation, Massachusetts Inst. Technol., Cambridge, MA, USA, 2007.

[57] J. Murota and T. Sawai, "Electrical characteristics of heavily arsenic and phosphorus doped polycrystalline silicon," *J. Appl. Phys.*, vol. 53, no. 5, pp. 3702–3708, May 1982.

[58] W. G. Spitzer, F. A. Trumbore, and R. A. Logan, "Properties of heavily doped *n*-type germanium," *J. Appl. Phys.*, vol. 32, pp. 1822–1830, Oct. 1961.

[59] Y. Furukawa, "Electrical properties of heavily doped n-type germanium," *J. Phys. Soc. Jpn.*, vol. 16, no. 4, pp. 687–694, Apr. 1961.

[60] V. V. Gavrushko, A. S. Ionov, V. A. Lastkin, and I. S. Telina, "On refractive index of optical radiation of polycrystalline silicon films," *J. Phys., Conf.*, vol. 1658, Oct. 2020, Art. no. 012016.

[61] Y. Laghla and E. Scheid, "Optical study of undoped, B or P-doped polysilicon," *Thin Solid Films*, vol. 306, no. 1, pp. 67–73, Aug. 1997.

[62] R. Pierret, *Advanced Semiconductor Fundamentals*, 2nd ed. London, U.K.: Pearson, Aug. 2002.

[63] H. Shen and F. H. Pollak, "Generalized Franz–Keldysh theory of electromodulation," *Phys. Rev. B, Condens. Matter*, vol. 42, no. 11, pp. 7097–7102, Oct. 1990.

[64] Y. Luo, J. Simons, J. Costa, I. Shubin, W. Chen, B. Frans, M. Robinson, R. Shafiiha, S. Liao, N.-N. Feng, X. Zheng, G. Li, J. Yao, H. Thacker, M. Asghari, K. Goossen, K. Raj, A. V. Krishnamoorthy, and J. E. Cunningham, "Experimental studies of the Franz–Keldysh effect in CVD grown GeSi epi on SOI," in *Proc. SPIE*, vol. 7944, pp. 169–183, 2011.

[65] S. Jongthammanurak, J. Liu, K. Wada, D. D. Cannon, D. T. Danielson, D. Pan, L. C. Kimerling, and J. Michel, "Large electro-optic effect in tensile strained Ge-on-Si films," *Appl. Phys. Lett.*, vol. 89, no. 16, Oct. 2006, Art. no. 161115.

[66] D. A. B. Miller, "Energy consumption in optical modulators for interconnects," *Opt. Exp.*, vol. 20, no. 2, p. A293, Mar. 2012.

[67] P. Chaisakul, D. Marris-Morini, M.-S. Rouifed, G. Isella, D. Chrastina, J. Frigerio, X. Le Roux, S. Edmond, J.-R. Coudevylle, and L. Vivien, "23 GHz Ge/SiGe multiple quantum well electro-absorption modulator," *Opt. Exp.*, vol. 20, no. 3, pp. 3219–3224, 2012.

[68] P. Chaisakul, D. Marris-Morini, G. Isella, D. Chrastina, X. Le Roux, S. Edmond, E. Cassan, J.-R. Coudevylle, and L. Vivien, "Ge/SiGe multiple quantum well photodiode with 30 GHz bandwidth," *Appl. Phys. Lett.*, vol. 98, no. 13, Mar. 2011, Art. no. 131112.

[69] P. Xu, Y. Zhang, S. Zhang, Y. Chen, and S. Yu, "SiN_x-Si interlayer coupler using a gradient index metamaterial," *Opt. Lett.*, vol. 44, no. 5, pp. 1230–1233, 2019.

[70] R. Konoike, K. Suzuki, K. Tanizawa, S. Suda, H. Matsuura, S. Namiki, H. Kawashima, and K. Ikeda, "SiN/Si double-layer platform for ultralow-crosstalk multiport optical switches," *Opt. Exp.*, vol. 27, no. 15, pp. 21130–21141, 2019.

NATDANAI KHONGPETCH received the Bachelor of Science degree (Hons.) in physics from Kasetsart University, in 2020, where he is currently pursuing the Graduate degree with the Department of Physics. His research interests include FDTD investigation on integrated optics and an electro-absorption modulator.

WORAWAT TRAIWATTANAPONG received the M.Sc. degree in physics from Kasetsart University, where he is currently pursuing the Ph.D. degree in physics with the Faculty of Science with a focus on low-energy germanium-silicon-based photonic devices. He has worked on vacancy defects and small polaron in barium titanate (BaTiO3) perovskite during his M.Sc. degree. He is also a visiting Student with the Department of Materials Science and Engineering, Massachusetts Institute of Technology (MIT), USA.

SURASAK CHIANGGA received the B.Sc. degree in physics from Srinakarinwirote University, in 1986, the M.Sc. degree in physics from Chulalongkorn University, Thailand, in 1993, and the Ph.D. degree in physics from the University of Innsbruck, Austria, in 1999. He is currently an Associate Professor with the Department of Physics, Kasetsart University. He has coauthored more than 59 refereed scientific papers. His research interests include nonlinear effects in silicon photonics, experimental quantum optics, and fabrication of nanomaterials.

PICHET LIMSUWAN received the B.Sc. degree in physics from Chulalongkorn University, in 1969, and the Ph.D. degree in physics from The Pennsylvania State University, USA, in 1978. He is currently a full Professor with the Department of Physics, Faculty of Science, King Mongkut's Institute of Technology Ladkrabang. He has coauthored more than 200 refereed scientific papers. His research interests include laser, thin films, and optical and nanomaterials.

PAPICHAYA CHAISAKUL received the bachelor's and master's degrees in electrical engineering from Chulalongkorn University, in 2004 and 2006, respectively, the dual M.Sc. degree in applied physics from École normale supérieure Paris-Saclay (École normale supérieure de Cachan) and the University of Wrocław, in 2009, and the Ph.D. degree in physics from Université Paris-Saclay (Université Paris-Sud), France, in 2012. He is currently an Associate Professor with the Department of Physics, Faculty of Science, Kasetsart Univerity. He has coauthored more than 70 refereed scientific papers. His research interests include silicon-based integrated optics for optical interconnect and sensing.